Limited ER quality control for GPI-anchored proteins

Natalia Sikorska,[1]* Leticia Lemus,[1]* Auxiliadora Aguilera-Romero,[4,5] Javier Manzano-Lopez,[2,3] Howard Riezman,[4,5] Manuel Muñiz,[2,3] and Veit Goder[1]

[1]Department of Genetics and [2]Department of Cell Biology, University of Seville, 41012 Seville, Spain
[3]Instituto de Biomedicina de Sevilla, Hospital Universitario Virgen del Rocío, Consejo Superior de Investigaciones Científicas, University of Seville, 41013 Seville, Spain
[4]National Centre of Competence in Research, Chemical Biology and [5]Department of Biochemistry, Sciences II, University of Geneva, 1211 Geneva 4, Switzerland

Endoplasmic reticulum (ER) quality control mechanisms target terminally misfolded proteins for ER-associated degradation (ERAD). Misfolded glycophosphatidylinositol-anchored proteins (GPI-APs) are, however, generally poor ERAD substrates and are targeted mainly to the vacuole/lysosome for degradation, leading to predictions that a GPI anchor sterically obstructs ERAD. Here we analyzed the degradation of the misfolded GPI-AP Gas1* in yeast. We could efficiently route Gas1* to Hrd1-dependent ERAD and provide evidence that it contains a GPI anchor, ruling out that a GPI anchor obstructs ERAD. Instead, we show that the normally decreased susceptibility of Gas1* to ERAD is caused by canonical remodeling of its GPI anchor, which occurs in all GPI-APs and provides a protein-independent ER export signal. Thus, GPI anchor remodeling is independent of protein folding and leads to efficient ER export of even misfolded species. Our data imply that ER quality control is limited for the entire class of GPI-APs, many of them being clinically relevant.

Introduction

Proteins of the secretory pathway are often modified after translocation across or insertion into the membrane of the ER (Braakman and Bulleid, 2011). A subclass of proteins that are to be targeted to the cell surface are attached to a specific membrane-embedded glycolipid, the GPI anchor (Mayor and Riezman, 2004). After attachment, the GPI anchor is subject to a series of remodeling steps on both its lipid and sugar moieties. In yeast, remodeling occurs exclusively inside the ER (Fig. 1). The sequential actions of the lipid remodeling enzymes Bst1, Per1, Gup1, and Cwh43 catalyze the addition of a long unsaturated fatty acid at the sn-2 position of the diacylglycerol (DAG) of the GPI anchor or, in most cases, the exchange of the DAG for ceramide (Reggiori et al., 1997; Umemura et al., 2007; Fujita and Kinoshita, 2012). In addition, the phosphoethanolamine from the second mannose of the GPI anchor is removed by the sugar remodeling enzyme Ted1, which promotes binding of GPI-anchored proteins (GPI-APs) to the receptor p24 complex for vesicular export from the ER (Fujita et al., 2009; Fujita and Kinoshita, 2012; Manzano-Lopez et al., 2015). In mammalian cells, GPI anchor remodeling inside the ER is catalyzed by PGAP1 (Bst1) and PGAP5 (Ted1), the latter of which promotes ER export analogous to yeast, whereas additional lipid remodeling occurs inside the Golgi (Tashima et al., 2006; Fujita and Jigami, 2008; Fujita et al., 2009).

If proteins to be exported from the ER fail to acquire their native fold, they are efficiently retained inside the ER by quality control mechanisms. Ultimately, they will be retrotranslocated and/or extracted from the membrane into the cytosol and targeted to the proteasome for degradation, a process called ER-associated degradation (ERAD; Meusser et al., 2005; Vembar and Brodsky, 2008). The Hrd1 complex is one of several conserved ERAD machineries in the ER and promotes the degradation of misfolded ER luminal and membrane proteins (Carvalho et al., 2006; Gauss et al., 2006; Mehnert et al., 2010). Interestingly, ER export can compete with retention mechanisms, as illustrated by findings that selected ERAD model substrates leave the ER to a significant extent if ER export signals are appended or upon overexpression (Haynes et al., 2002; Spear and Ng, 2003; Kincaid and Cooper, 2007). The eukaryotic cell possesses additional protein quality control mechanisms in the secretory pathway downstream of the ER; these mechanisms target substrates to the proteasome independently of ERAD or to the vacuole/lysosome (Arvan et al., 2002; Wang and Ng, 2010; Zhao et al., 2013).

Because of the roles of GPI-APs in prominent human diseases, including malaria (Davidson and Gowda, 2001) and neurodegenerative prion diseases (Puig et al., 2014; Victoria and Zurzolo, 2015), the intracellular quality control of selected GPI-

*N. Sikorska and L. Lemus contributed equally to this paper.

Correspondence to Veit Goder: vgoder@us.es

N. Sikorska's present address is Institut de Biologie Moléculaire des Plantes du Centre National de la Recherche Scientifique, University of Strasbourg, 67081 Strasbourg, France.

Abbreviations used in this paper: CHX, cycloheximide; coIP, coimmunoprecipitation; DAG, diacylglycerol; ERAD, ER-associated degradation; ERES, ER exit site; GPI-AP, GPI-anchored protein; PI-PLC, phosphoinositol-specific phospholipase C; TAP, tandem affinity purification; TMD, transmembrane domain; UPR, unfolded protein response.

The Rockefeller University Press $30.00
J. Cell Biol. Vol. 213 No. 6 693–704
www.jcb.org/cgi/doi/10.1083/jcb.201602010

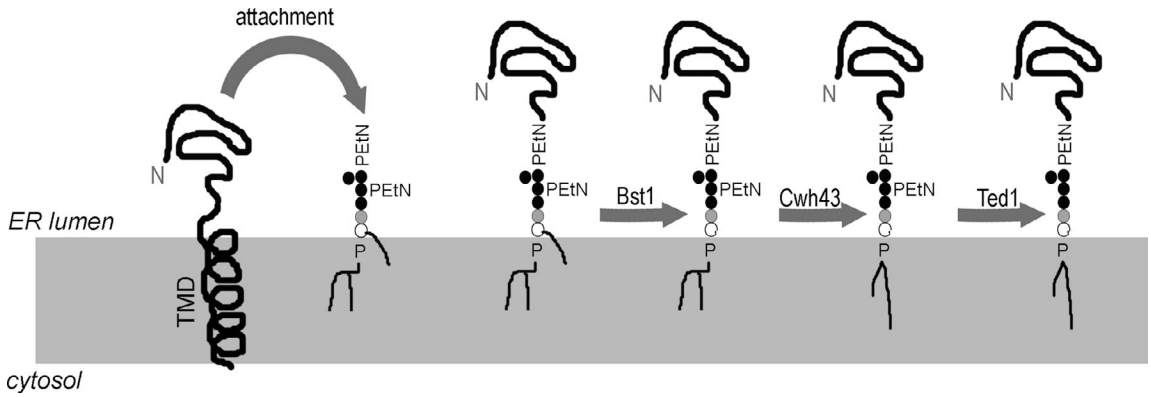

Figure 1. **GPI anchor remodeling in the yeast ER.** After translocation into the ER, the C-terminal TMD is removed and the luminal part of the protein is attached to a GPI anchor via a phosphoethanolamine (PEtN). After attachment, the sugar and lipid moieties of the GPI anchor undergo remodeling. Bst1 removes the acyl chain from the inositol (open circle), a step required for downstream lipid remodeling. Cwh43 exchanges the diacylglycerol for ceramide, the major lipid on remodeled GPI anchors in yeast. For simplicity, Per1 and Gup1, which catalyze intermediate lipid remodeling steps, are not shown. Ted1 removes a PEtN on the second mannose (closed circles), enabling efficient binding to the p24 complex for ER export.

APs has been studied extensively. Various misfolded GPI-APs accumulate in the presence of proteasome inhibitors, suggesting that ERAD is involved in their turnover (Ma and Lindquist, 2001; Yedidia et al., 2001; Petris et al., 2014; Wang et al., 2014). However, this view was challenged by the observation that the proteasome also degrades nontranslocated species, and recent studies suggested that ER-localized misfolded GPI-APs are predominantly routed to lysosomes for degradation (Drisaldi et al., 2003; Ashok and Hegde, 2008; Satpute-Krishnan et al., 2014).

Recent work with yeast to study the quality control of misfolded GPI-APs centered on Gas1*, a mutant version of the β-1,3-glucanosyltransferase Gas1, which normally functions in cell wall assembly. Gas1* contains a single point mutation (G291R) that renders the protein unstable and leads to its degradation (Fujita et al., 2006). Subsequent work showed that, like degradation of misfolded GPI-APs in mammalian cells, only a minor fraction of Gas1* was routed to ERAD, whereas most of its degradation depended on ER export and probably occurred inside the vacuole, although evidence for vacuolar degradation of Gas1* is still lacking (Fujita et al., 2006; Hirayama et al., 2008; Goder and Melero, 2011).

Altogether, these data suggest that misfolded GPI-APs are generally rather poor ERAD substrates, but the reasons for this phenomenon are unclear. Interestingly, misfolded mutant versions of the prion protein could be efficiently routed to ERAD when GPI anchor attachment was prevented (Ashok and Hegde, 2008). In combination with a more recent study, this result led to the postulation that the presence of a GPI anchor might generally obstruct ERAD for sterical reasons (Satpute-Krishnan et al., 2014). However, this would be in conflict with the observation that at least a minor fraction of Gas1* in yeast is a substrate for Hrd1-dependent ERAD (Goder and Melero, 2011). To address these uncertainties and the mechanisms that determine the degradation pathways of misfolded GPI-APs, we performed a detailed analysis of the degradation of the misfolded GPI-AP Gas1* in yeast.

Results

We have previously shown that Gas1* can be degraded by several cellular pathways in parallel, including Hrd1-dependent ERAD and post-ER degradation involving ER export that is dependent on the p24 protein complex component Emp24 (Goder and Melero, 2011). Although *Δhrd1Δemp24* cells showed stronger stabilization of Gas1* than individual single mutants, suggesting that ER-exported Gas1* was not rerouted to the ER for ERAD, it was not clear whether Gas1* was ultimately targeted to the vacuole (Goder and Melero, 2011). Indeed, earlier results showed that Gas1* was not stabilized in a *Δpep4* mutant, in which vacuolar proteases are inactive (Fujita et al., 2006). When we expressed HA-tagged Gas1* (HA-Gas1*) and measured protein turnover using the translation elongation inhibitor cycloheximide (CHX) in wild-type cells and *Δpep4* cells, we obtained similar results, with no visible protein stabilization in the *Δpep4* mutant (Fig. 2, A [lanes 1–9] and B). However, when we measured the effect of *Δpep4* deletion in the *Δhrd1* background, which on its own showed only marginal Gas1* stabilization, we found a significant increase in protein stability compared with the individual single mutants, showing that a fraction of Gas1* is routed to the vacuole for degradation (Fig. 2, A [lanes 10–18] and B). These data reinforce the idea that Gas1* can be degraded dynamically by several simultaneously operating degradation pathways, one of them being ERAD and another depending on ER export and leading to the vacuole (Fig. 2 C). These results also explain why blockage of only one of these pathways in single mutants might not (necessarily) be sufficient to significantly reduce the global degradation rate.

Important for resolving whether a GPI anchor obstructs ERAD is to determine whether Gas1* routed to this pathway contains a GPI anchor or still a transmembrane domain (TMD; Fig. 2 C, dashed arrows). To address this, we were initially looking for mutants in which the routing of Gas1* to the vacuole is reduced in favor of increased ERAD. We expressed a GFP-tagged version of Gas1* for a comparative analysis of protein targeting to the vacuole by live cell fluorescence microscopy (Fig. 3, A and B). Wild-type cells showed a strong vacuolar signal, in agreement with a significant fraction of Gas1* being routed to the vacuole despite ERAD being fully operational (Fig. 3 B, wild type). The faint perivacuolar puncta could be post-ER trafficking intermediates (Fig. 3 B, wild type). In the absence of the p24 complex component Emp24, when GPI-AP–specific ER export is impaired and Gas1* degradation is reduced (Muñiz et al., 2000; Goder and Melero, 2011), the vacuolar signal was decreased and the perinuclear and cortical

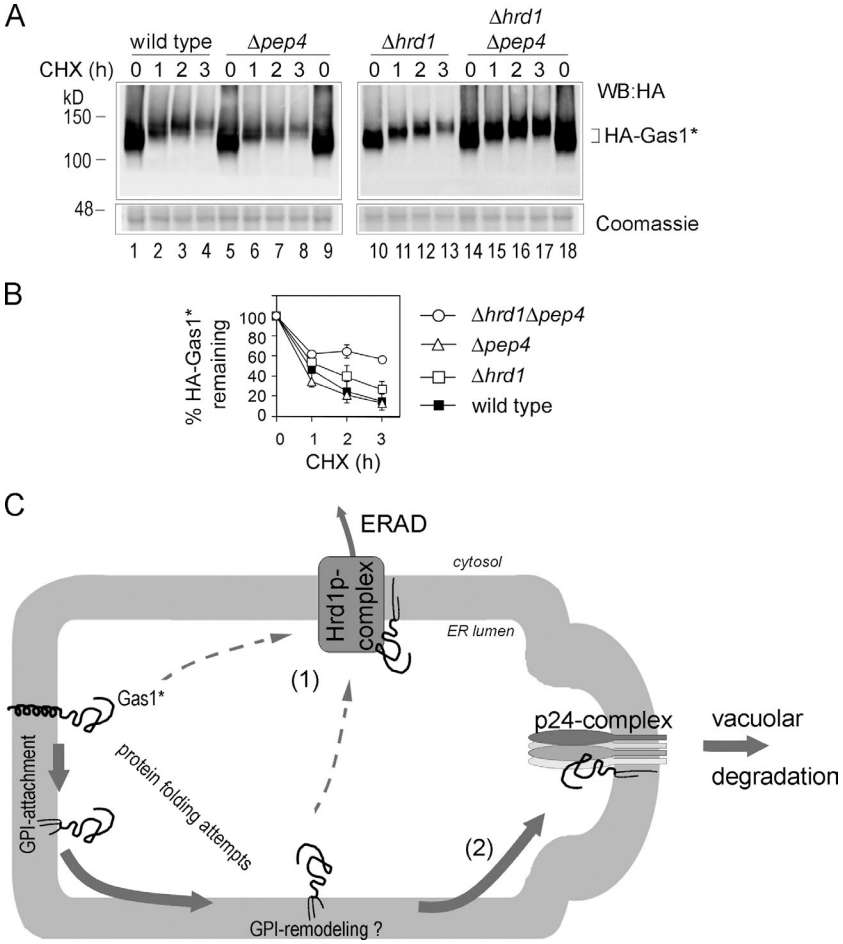

Figure 2. **Dynamic routing of the misfolded GPI-AP Gas1* to ERAD and/or the vacuole for degradation.** (A) Wild-type cells and the indicated single and double mutant cells expressing HA-Gas1* were subjected to CHX shut-off experiments. Cells were lysed, and the remaining HA-Gas1* was measured by SDS-PAGE and Western blotting (WB) with antibodies against HA. Accumulation of higher-molecular-weight species during chase periods is caused by protein *O*-mannosylation (Goder and Melero, 2011). A lower part of the gel was separately stained with Coomassie as loading control. (B) Quantifications of results from experiments shown in A. Mean values and SDs from at least three individual experiments are shown. (C) Schematic representation of the degradation pathways of Gas1* in wild-type cells. (1) A fraction of Gas1* is routed to the Hrd1-dependent ERAD machinery, retrotranslocated, and degraded by the proteasome (not shown). It is unclear whether Gas1* can be routed to ERAD only before or also after attachment to the GPI anchor (dashed lines). (2) A larger fraction of Gas1* is exported from the ER and routed to the vacuole for degradation. ER export of Gas1* depends in part on the p24 complex, but it is unknown whether and to what extent the GPI anchor of Gas1* is remodeled.

ER was stained more strongly, suggesting a reduction in ER export of GFP-Gas1* (Fig. 3 B, *Δemp24*). A similar phenotype was seen in the absence of the GPI anchor remodeling enzyme Ted1, which acts immediately upstream of Emp24 (Fig. 3 B, *Δted1*). The fact that *Δted1* cells phenocopied *Δemp24* cells suggests that the GPI anchor of Gas1* undergoes sugar remodeling. Remaining vacuolar staining likely arises from the ER export of GPI-APs by bulk-flow mechanisms (Manzano-Lopez et al., 2015). Cells with deleted Hrd1, lacking Hrd1-dependent ERAD, showed vacuolar staining similar to that of wild-type cells (Fig. 3 B, *Δhrd1*). Increased staining of the perinuclear ER in *Δhrd1* cells compared with wild-type cells might reflect elevated nonspecific ER retention of misfolded proteins by the up-regulated unfolded protein response (UPR) in this ERAD mutant (Jonikas et al., 2009). However, UPR activation does not cause the major differences in Gas1* ER export in the distinct mutants, because the UPR is less elevated in *Δted1* cells than in *Δhrd1* cells (Jonikas et al., 2009). To quantify the differences in GFP-Gas1* targeting to the vacuole in the distinct mutants, we measured free GFP that resisted vacuolar proteolysis as a remnant of GFP-Gas1*. Free GFP was reduced up to 50% in *Δemp24* and in *Δted1* cells compared with wild-type and *Δhrd1* cells (Fig. 3, C and D).

Next we tested whether more Gas1* was routed to ERAD in *Δemp24* and *Δted1* cells compared with wild-type cells. We expressed HA-tagged Gas1* and measured protein turnover using CHX. Deletion of *HRD1* in the *Δted1* or *Δemp24* background showed a much stronger stabilizing effect than the *HRD1* deletion in wild-type cells (Fig. 3, E–G). Quantification revealed that ERAD is the major degradation pathway for Gas1* in *Δemp24* and in *Δted1* cells, with more than 50% of protein turnover being dependent on Hrd1 (Fig. S1).

Next, we measured the amount of cellular Gas1* that contained a GPI anchor under these conditions. We used phosphoinositol-specific phospholipase C (PI-PLC), which cleaves the phosphate diester of the GPI anchor at the sn-3 position, thereby removing the lipophilic DAG or ceramide and rendering a GPI-AP water soluble. In combination with Triton X-114 phase separation, we found that more than 90% of HA-Gas1* was recovered in the aqueous phase after treatment of lysates with PI-PLC, irrespective of the tested strain (Fig. 4, A and B, HA-Gas1*). As a control, we expressed HA-Gas1*TMD in *Δemp24* cells, a construct in which the exchange of the TM domain for the GPI anchor is prevented by a specific mutation (N528Q), therefore rendering HA-Gas1*TMD a type I TM protein. As expected, HA-Gas1*TMD was not recovered in the aqueous phase after PI-PLC treatment, validating the functionality of the assay (Fig. 4, A and B, HA-Gas1*TMD). This result shows that Gas1* is efficiently attached to a GPI anchor in all tested strains, including those in which >50% of Gas1* is routed to Hrd1-dependent ERAD. Therefore, the Hrd1-machinery can mediate ERAD of a misfolded GPI-AP.

Because our data ruled out that sterical obstructions limit ERAD of a misfolded GPI-AP, the question remained as to why misfolded GPI-APs are often exported from the ER and predominantly degraded inside the vacuole/lysosome. In striking resemblance to results obtained in mammalian cells with mutant prion proteins lacking the GPI anchor (Ashok and Hegde,

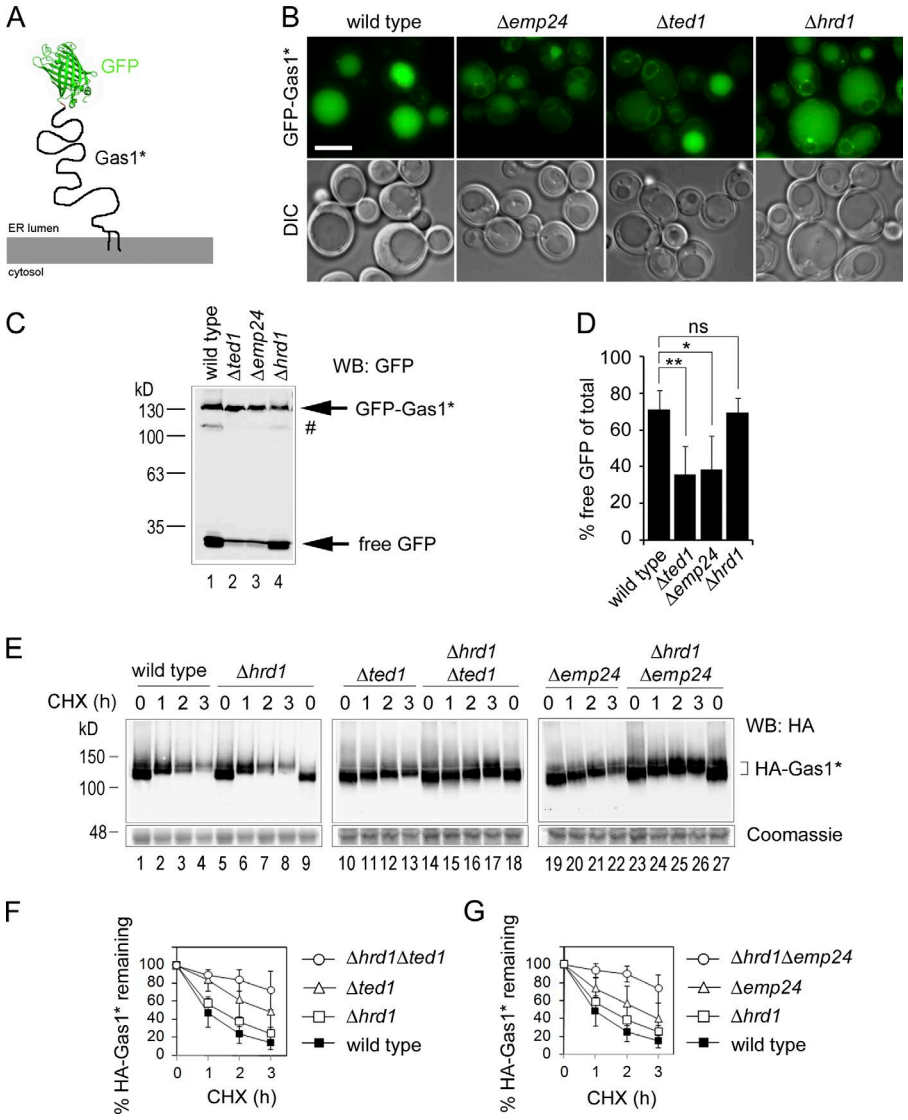

Figure 3. **Increased targeting of Gas1* to ERAD in *Δemp24* and *Δted1* cells.** (A) Schematic representation of the fusion construct GFP-Gas1*. The GFP moiety was fused to the N-terminus domain of Gas1*, downstream of the signal sequence. The C-terminal GPI anchor extends into the luminal leaflet of the ER membrane. (B) Wild-type and indicated mutant cells expressing GFP-Gas1* were analyzed by live cell fluorescence microscopy. DIC = Nomarski image. Bar, 2 µm. (C) GFP-cleavage assay. Cells used for microscopy in B were lysed in equal amounts and analyzed by SDS-PAGE in combination with Western blotting (WB) with antibodies against GFP. The hashtag indicates a minor fraction of the fusion protein that likely has not been translocated into the ER. (D) Quantification and statistical analysis of results from experiments shown in C. Mean values and SDs from at least three individual experiments are shown. ns, not significant. *, $P < 0.05$; **, $P < 0.01$ (unpaired two-tailed Student's *t* test). (E) Wild-type cells and the indicated single and double mutant cells expressing HA-Gas1* were subjected to CHX shut-off experiments. A lower part of the gel was separately stained with Coomassie as loading control. (F and G) Quantifications of results from experiments shown in E. Mean values and SDs from at least three individual experiments are shown.

2008), we found that significantly less GFP-Gas1*TMD was targeted to the vacuole and more retained inside the ER compared with GFP-Gas1* in wild-type cells, as shown by fluorescence microscopy (Fig. 5 A). Similar results were obtained with GFP-Gas1*ΔTMD, in which the C-terminal TMD was deleted, rendering the construct a soluble ER luminal

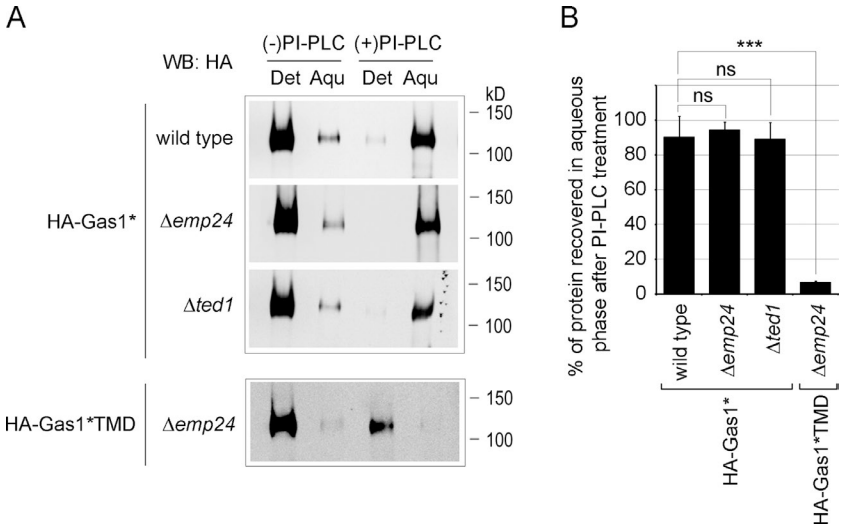

Figure 4. **Gas1* is efficiently attached to the GPI anchor.** (A) Triton X-114 extracts from wild-type cells and the indicated single mutant cells expressing HA-Gas1* or HA-Gas1*TMD were treated with PI-PLC or mock-treated. Detergent (Det) and aqueous (Aqu) phases were separated and analyzed by SDS-PAGE and Western blotting (WB) with antibodies against HA. (B) Quantification of the relative amounts of HA-Gas1* and HA-Gas1*TMD recovered in the aqueous phase compared with total signal after treatment with PLC from experiments shown in A. Mean values and SDs from two to five individual experiments are shown. ns, not significant. ***, $P < 0.001$ (unpaired two-tailed Student's *t* test).

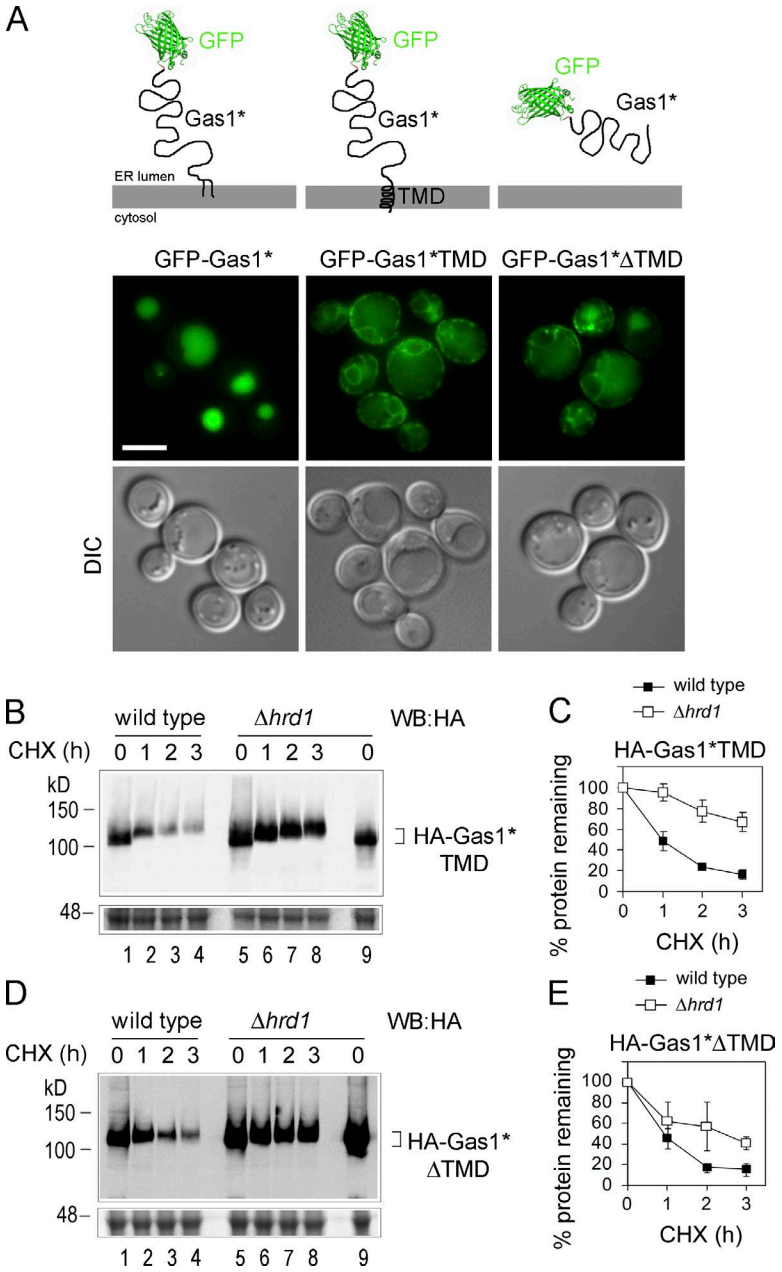

Figure 5. **Preventing GPI anchor attachment increases ER retention and routing of Gas1* to ERAD.** (A) Live cell fluorescence microscopy of wild-type cells expressing the indicated GFP-Gas1* fusion constructs. Schematic illustrations of the various constructs are shown above the microscopy images. DIC = Nomarski image. Bar, 2 µm. (B–E) Wild-type cells and *Δhrd1* cells expressing HA-Gas1*TMD and HA-Gas1*ΔTMD were subjected to CHX shut-off experiments. A lower part of the gel was separately stained with Coomassie as loading control. The graphs illustrate the obtained degradation rates and show the mean values and SDs from at least three individual experiments.

misfolded protein (Fig. 5 A). In addition, the stabilizing effect of the Hrd1 deletion was significantly larger for the HA-tagged versions of both constructs lacking the GPI anchor compared with HA-Gas1* (Fig. 5, B and C, versus Fig. 3, E and F). In light of these data, it appears that a GPI anchor reduces the routing of misfolded proteins to ERAD by limiting ER retention or by promoting ER export.

Recent data suggested that GPI-APs would mix with free ceramides inside the ER and promote the cotransport of free ceramides in vesicles from the ER to the Golgi (Loizides-Mangold et al., 2012). We considered the possibility that Gas1*, albeit misfolded, would function in ceramide cotransport by virtue of its GPI anchor. Such a function could bypass ER-retention mechanisms and explain the universally observed reduction in ERAD. However, a combination of experiments, including lipid analysis in which we determined the ceramide and sphingolipid profiles of *Δgas1* cells expressing HA-Gas1 or HA-Gas1* or the anchorless versions HA-Gas1TMD and HA-Gas1*TMD, did not provide any evidence for a role of Gas1* in ceramide cotransport (Fig. S2).

It has been shown that ER export of (correctly folded) GPI-APs is directly coupled to GPI anchor remodeling (Castillon et al., 2009, 2011; Fujita et al., 2009; Manzano-Lopez et al., 2015). In fact, the remodeled GPI anchor is the major, if not the only, ER export signal of GPI-APs. GPI anchor lipid remodeling promotes the concentration of GPI-APs in specific ER exit sites (ERESs) where binding to the p24 complex is thought to occur (Castillon et al., 2009). p24 proteins can bind to synthetic remodeled but not unremodeled glycostructures of the GPI anchor and to specific sphingolipids that contain ceramide, a lipid also present in remodeled GPI anchors (Contreras et al., 2012; Manzano-Lopez et al., 2015). The observed reduction in ER export of Gas1* in *Δted1* cells indicates that its GPI anchor undergoes sugar remodeling (Fig. 3, E and F). To test whether the GPI anchor of Gas1* undergoes lipid remodeling as well, we used a flotation assay (Castillon et al., 2011). HA-Gas1*

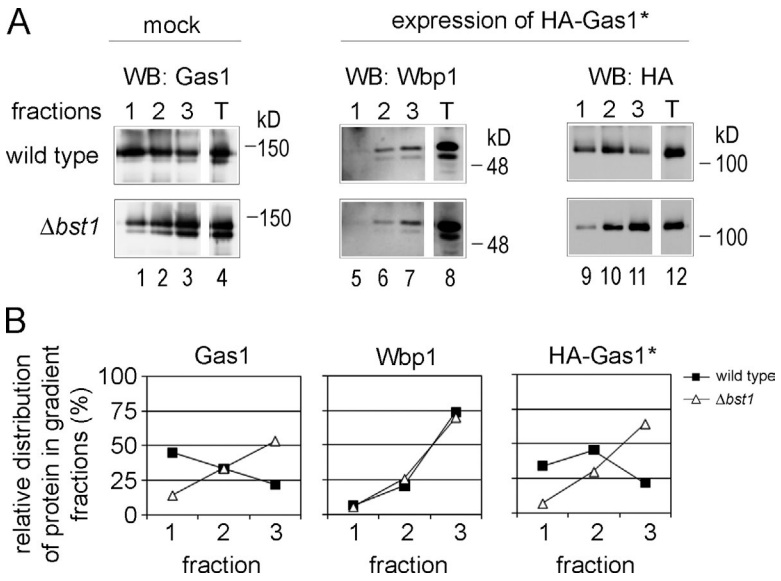

Figure 6. **The GPI anchor of Gas1* undergoes lipid remodeling.** (A) Lysates of wild-type cells and *Δbst1* cells with or without expression of HA-Gas1* were subjected to flotation in an Optiprep gradient. The three top fractions of the gradient as well as the total (T) were analyzed by SDS-PAGE and Western blotting (WB) with the indicated antibodies. (B) Graphical display of the results shown in A. The relative distribution of each individually analyzed protein in the three top fractions is plotted after quantifying protein bands from the WBs shown in A.

and Gas1, but not the control TM protein Wbp1, were recovered in the top gradient fractions (fraction 1), indicating the presence of a long-chain fatty acid that promotes association with membrane rafts (Fig. 6, A and B, wild type). The amount of HA-Gas1* and Gas1 in the top gradient fractions was strongly reduced in *Δbst1* cells, in which lipid remodeling of the GPI anchor is blocked genetically, indicating that the GPI anchor of Gas1* was lipid-remodeled in wild-type cells (Fig. 6, A and B, *Δbst1*). Thus, Gas1*, like Gas1, undergoes sugar and lipid remodeling. This scenario could explain why Gas1*, despite being misfolded, is efficiently exported from the ER although being a substrate for ERAD.

To investigate this further, we tested whether inhibition of GPI anchor remodeling would increase the routing of Gas1* to ERAD. This was true for *Δted1* cells, where sugar remodeling is blocked (Fig. 3, E and F). We extended this test and measured the degradation of Gas1* in the lipid-remodeling mutants *Δbst1* and *Δcwh43*. The global degradation rate of HA-Gas1* was not affected in the single mutants (Fig. 7, A and D). However, expression of GFP-Gas1* revealed that less protein was routed to the vacuole and more was retained inside the ER in both mutants compared with wild-type cells (Fig. 7 B). At the same time, more Gas1* was now degraded by ERAD, because *Δhrd1Δbst1* and *Δhrd1Δcwh43* double mutants showed a marked increase in protein stability compared with the individual single mutants (Fig. 7, C and D). Conversely, Gas1* degradation was not affected when Emp24-dependent export was blocked in the same mutants, consistent with the predominant routing of Gas1* to ERAD (Fig. 7, E and F). Interestingly, *Δemp24Δbst1* and *Δemp24Δcwh43* mutants showed faster Gas1* turnover than *Δemp24* cells (Fig. 7 E). This could indicate that routing of GPI-APs to ERAD is more efficient for GPI-APs that are not yet lipid-remodeled compared with lipid-remodeled species that accumulate in *Δemp24* cells. It is known that lipid-remodeled species tend to localize to membrane rafts and to GPI-AP–specific ERESs (Castillon et al., 2011), which might be less accessible for the ERAD machinery. This could explain why the global degradation rate of Gas1* is decreased in *Δemp24* and, analogously, in *Δted1* cells, compared with *Δbst1* or *Δcwh43* cells (compare Fig. 7 A with Fig. 3 E). Future studies will address these questions in detail.

To address the mechanism of ER export of Gas1*, we assayed its binding to the p24 complex component Emp24. Binding of a GPI-AP to Emp24 was previously shown to depend on anchor remodeling (Castillon et al., 2011; Manzano-Lopez et al., 2015). Using tandem affinity purification (TAP)-tagged Emp24, we could efficiently coimmunoprecipitate (coIP) the ER form of HA-Gas1* (Fig. 8 A, lane 12). Importantly, the efficiency of coIP was comparable to that of Gas1, supporting the conclusion that the GPI anchor was remodeled independently of protein folding (Fig. 8 A, compare lanes 10 and 12). The binding to the anchorless mutants HA-Gas1*TMD and HA-Gas1TMD was strongly reduced, confirming that the interaction between Gas1 or Gas1* and Emp24 was mainly GPI anchor dependent (Fig. 8 A, lanes 14 and 16; Castillon et al., 2011). Interestingly, higher-molecular-weight versions of Gas1* and Gas1 constructs, which correspond to forms that have undergone further glycosylation in the Golgi, were also immunoprecipitated with Emp24-TAP in a manner that was independent of the presence of the GPI anchor (Fig. 8, [post-]Golgi forms). This is in agreement with a proposed function of the p24 complex in retrieval of misfolded or incompletely remodeled GPI-APs from the Golgi to the ER by a mechanism that does not depend on anchor remodeling (Castillon et al., 2011).

Because a conserved mechanism for the ER export of GPI-APs in yeast and mammals consists of Ted1/PGAP5-mediated sugar remodeling of the GPI anchor, we tested whether binding of Gas1* to Emp24 was dependent on Ted1. Indeed, binding of the ER form of HA-Gas1* to Emp24-TAP was strongly reduced in *Δted1* cells, supporting the idea that ER exit of Gas1* is mediated by canonical GPI anchor remodeling that seemingly occurs irrespective of the state of protein folding (Fig. 8 B).

To generalize these findings, we performed additional experiments with an entirely distinct misfolded protein. We used CPY*, a mutant version of the soluble vacuolar carboxypeptidase Y and classic Hrd1-dependent ERAD substrate (Bordallo et al., 1998). To directly evaluate whether a GPI anchor would induce the targeting of CPY* to the vacuole, we generated the fusion proteins GFP-CPY*TMD and GFP-CPY*GPI, which differ only in the nature of their membrane anchors. Live cell fluorescence microscopy revealed that GFP-CPY*TMD, which lacks a GPI anchor, was retained rather efficiently inside the

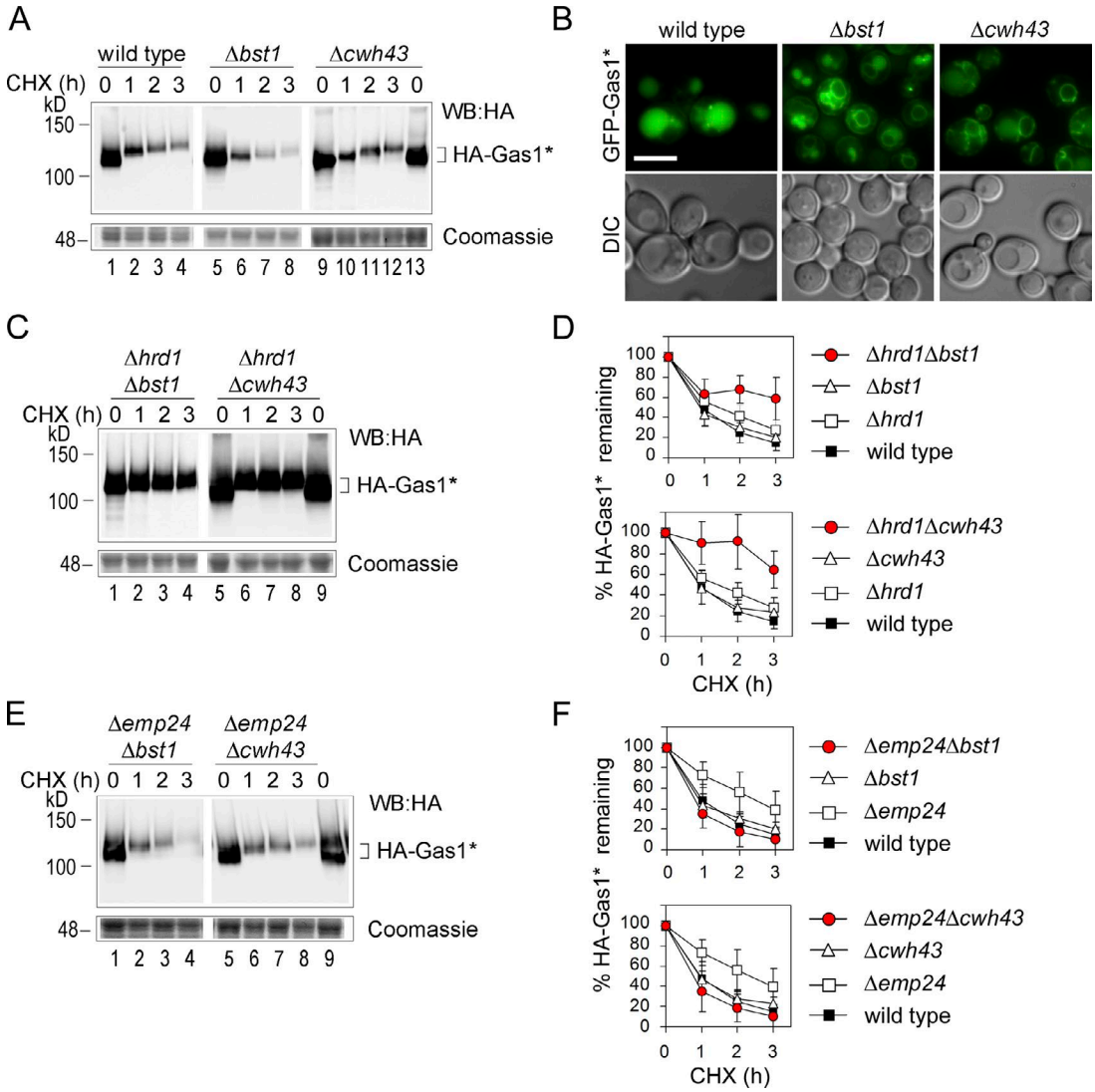

Figure 7. **Increased targeting of Gas1* to ERAD in GPI anchor lipid remodeling mutants.** (A) CHX shut-off experiments with wild-type cells and remodeling mutants expressing HA-Gas1*. The lower part of the gel was separately stained with Coomassie as loading control. (B) Live cell fluorescence microscopy with wild-type cells and remodeling mutants expressing GFP-Gas1*. DIC = Nomarski image. Bar, 3 µm. (C–F) CHX shut-off experiments with the indicated double mutants expressing HA-Gas1*. The lower parts of the gels were separately stained with Coomassie as loading control. For quantification and statistical analysis, results from experiments shown in A as well as from those shown in Fig. 3 E (*Δhrd1* and *Δemp24* cells) were used. Mean values and SDs from at least three individual experiments are shown. Red circles are used to highlight the degradation rates in the double mutants.

ER, with only weak vacuolar signal, indicating minor trafficking to the vacuole (Fig. 9 A, GFP-CPY*TMD). In contrast, the attachment of the GPI anchor resulted in a prominent vacuolar signal and reduced ER membrane staining, indicating increased targeting to the vacuole of this construct (Fig. 9 A, GFP-CPY*GPI). Moreover, the GFP cleavage assay revealed a significant increase in the production of free GFP with GFP-CPY*GPI in comparison to GFP-CPY*TMD, showing that the presence of the GPI anchor led to a global increase in vacuolar degradation of the CPY* fusion protein (Fig. 9, B [compare lanes 1 and 3] and C). The near-absence of free GFP when the same constructs were expressed in the *Δpep4* strain confirmed that free GFP produced in wild-type cells originated from the vacuole (Fig. 9, B [compare lanes 1 and 3 with lanes 2 and 4] and C). In addition to an increase in vacuolar degradation in the presence of the GPI anchor, measurements of Hrd1-dependent degradation using HA-tagged versions of the fusion constructs revealed that the exchange of a TMD for a GPI anchor resulted in a significant drop in ERAD (Fig. 9, D and E). Together, the data obtained with CPY* corroborate those obtained with Gas1* and show that the presence of a GPI anchor on a misfolded ER protein generally causes a reduction in ER retention and ERAD in favor of an increase in ER export, followed by ultimate degradation inside the vacuole.

Discussion

Our data demonstrate that a GPI anchor does not pose a sterical obstruction for the degradation of a misfolded GPI-AP through a canonical ERAD pathway. In contrast to degradation of a misfolded GPI-AP inside the vacuole, where the GPI anchor may be removed by lipases and/or glycosidases, degradation of the same substrate through ERAD hints at the existence of a

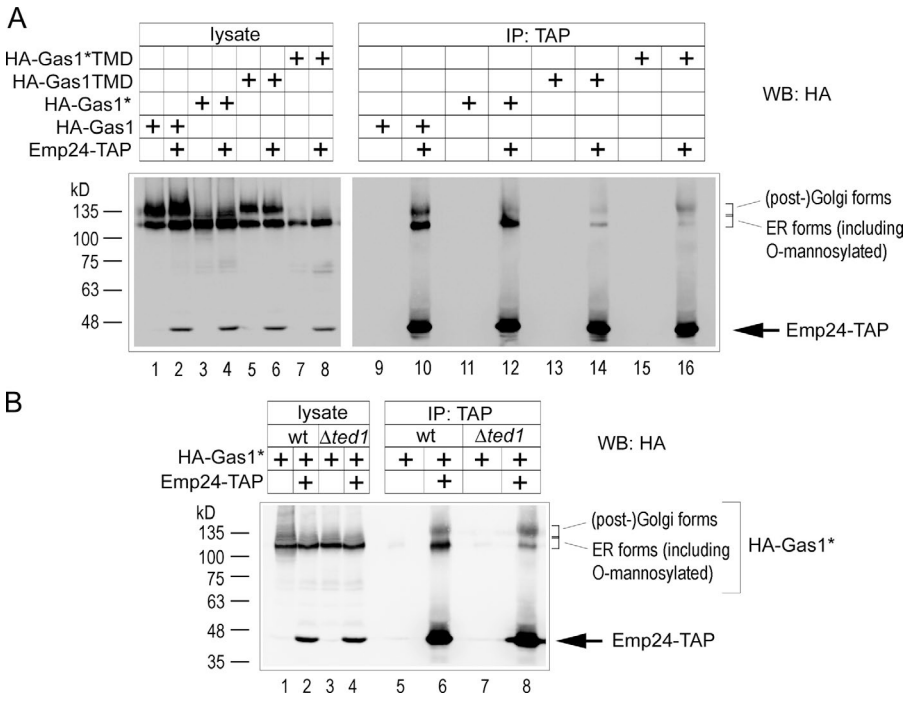

Figure 8. **GPI anchor remodeling-dependent binding of Gas1* to Emp24.** (A) Wild-type cells coexpressing chromosomally TAP-tagged Emp24 and the indicated Gas1 or Gas1* constructs and control cells were subjected to co-immunoprecipitation (IP) experiments followed by SDS-PAGE and Western blotting (WB) with antibodies against HA. Emp24-TAP was recognized by the secondary antibody. (B) As in A, with wild-type cells and *Δted1* cells coexpressing Emp24-TAP and HA-Gas1* or control cells.

yet-unknown cellular mechanism for the removal of the GPI anchor during or after protein retrotranslocation to allow degradation by the proteasome. The presence of such a mechanism is also implied by observation that other posttranslational protein modifications such as glycans on retrotranslocated proteins are removed by a conserved specific cytosolic glycanase before proteasomal degradation (Katiyar et al., 2004). We are currently pursuing the identification of cellular components involved in the removal of a GPI anchor during ERAD.

Remodeled GPI anchors on (correctly folded) GPI-APs were previously known to be recognized by the p24 complex ER export machinery, thereby connecting GPI anchor remodeling with ER export. Our finding that a GPI anchor is remodeled irrespective of protein (mis)folding reveals that a potent ER export signal is also generated on a misfolded protein. We furthermore showed that the remodeled GPI anchor of misfolded Gas1* promotes binding to Emp24, which suggests that inefficient ER retention and ERAD of the tested misfolded GPI-APs are a consequence of efficient GPI anchor–mediated ER export. Although we observed variations in the degree of ER retention, ERAD, and degradation inside the vacuole between different tested constructs, we found in all cases that the presence of a GPI anchor resulted in a larger fraction of the misfolded protein to be exported from the ER and routed to the vacuole compared with the same protein when membrane-anchored via a TMD or when soluble. These observations combined suggest that the ER residence time for misfolded GPI-APs is mainly determined by remodeling of the GPI anchor and only to a minor degree by protein folding.

On a speculative note, it could be possible that ER protein-retention mechanisms, which are largely based on protein–protein and protein–glycan interactions between substrates and chaperones, are in competition with lipid-based sorting mechanisms connected to membrane homeostasis or membrane traffic. For instance, the particular lipids that are part of the GPI anchor, in particular after anchor remodeling, are likely to affect ER membrane homeostasis at least locally and might necessitate efficient export from the ER (Copic et al., 2009). Alternatively, the known segregation of GPI-APs from other membrane and soluble proteins inside the ER as part of a sorting mechanism linked to membrane traffic might limit the access of misfolded GPI-APs to particular cellular components involved in ER retention and protein quality control (Muñiz et al., 2001; Castillon et al., 2009). Future work will address these possibilities.

Based on our results, we propose that canonical GPI anchor remodeling universally limits the ER quality control of GPI-APs. This provides a unifying model for the increasing number of observations in various organisms that misfolded GPI-APs are rather poor ERAD substrates. Interference with GPI anchor remodeling could thus also be a relevant approach in an attempt to increase ERAD of certain disease-prone mutant prion proteins that are converted into pathogenic aggregates only after ER exit (Victoria and Zurzolo, 2015). Finally, our data also illustrate the importance of post-ER quality control mechanisms, about which much is still to be learned, that have particular relevance for the entire class of GPI-APs.

Materials and methods

Yeast strains

A detailed list of yeast strains used in this study is found in Table S1.

Construction of plasmids

All constructs used in this study were expressed from integrative plasmids under the control of the endogenous *GAS1* promoter. Plasmid markers are indicated in the list of yeast strains (Table S1). The construct for the expression of HA-Gas1*, pMF616, was a gift from the Jigami laboratory (Fujita et al., 2006). A construct expressing HA-Gas1 was generated from pMF616 by changing the single point mutation (G291R) back to wild-type sequence using the primers 5′-GATGTC TGGTCTGGTGGTATCGTATACATGTAC-3′ and 5′-GTACATGTA TACGATACCACCAGACCAGACATC-3′ in combination with the Quikchange protocol from Agilent Technologies, yielding NSp17. To

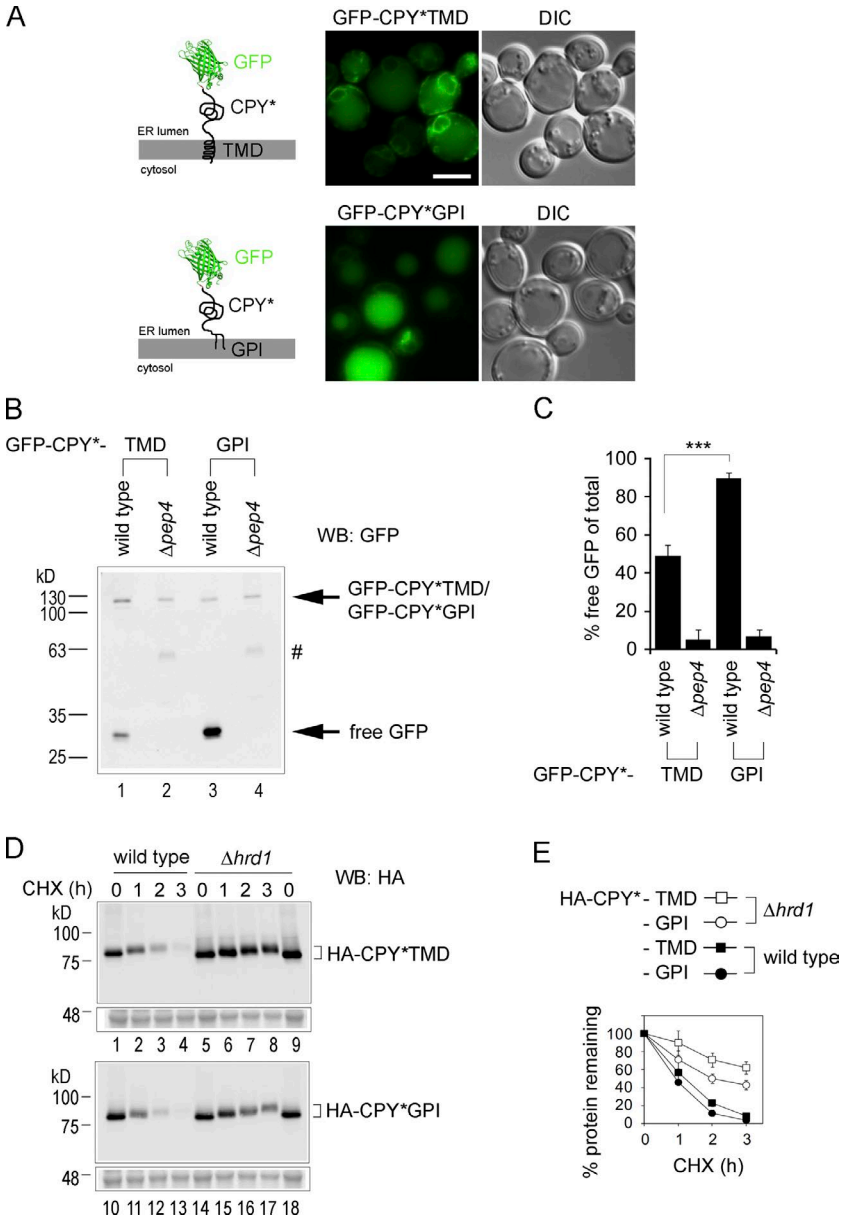

Figure 9. **The presence of a GPI anchor on CPY* causes an increase in vacuolar degradation and a parallel decrease in ERAD compared with CPY* with a TMD.** (A) Live cell fluorescence microscopy of wild-type cells expressing the indicated GFP-CPY* fusion constructs. Schematic illustrations of the various constructs are shown. From previously used GFP-Gas1* fusion constructs, the Gas1* moiety, with the exception of 57 amino acids comprising its C-terminal domain containing the GPI anchoring signal, was exchanged with CPY*; for details see Materials and methods. DIC = Nomarski image. Bar, 2 µm. (B) GFP-cleavage assay. Cells used for microscopy in A and *Δpep4* cells expressing the same constructs were lysed in equal amounts and analyzed by SDS-PAGE in combination with Western blotting (WB) with antibodies against GFP. The hashtag indicates a non-specific protein that accumulated in *Δpep4* cells. (C) Quantification and statistical analysis of results from experiments shown in B. Mean values and SDs from at least three individual experiments are shown. ***, $P < 0.001$ (unpaired two-tailed Student's *t* test). (D) Wild-type cells and the indicated mutant cells expressing HA-CPY*TMD and HA-CPY*GPI were subjected to CHX shut-off experiments. Protein *O*-mannosylation occurs within the serine-rich region proximal to the GPI anchoring site that is part of the C-terminal 57 amino acids of the fusion proteins that originate from Gas1 (Gatti et al., 1994). A lower part of the gel was separately stained with Coomassie as loading control. (E) Quantification of results from experiments shown in D. Mean values and SDs from at least three individual experiments are shown.

generate constructs for the expression of mutants lacking GPI anchors, the point mutations K526R and N528Q were simultaneously introduced into pMF616 and NSp17 using PCR-based single primer site-directed mutagenesis and the primer 5′-CAGCTTCATCTTCATCTTCTTCGC GAAAGCAAGCTGCCACCAACGTTAAAGC-3′, yielding NSp23 (HA-Gas1*TMD) and NSp20 (HA-Gas1TMD). To generate the soluble version HA-Gas1*ΔTMD, a stop codon was introduced into the coding region of the protein just upstream of the TMD using the same method in combination with pMF616 as template and the primer 5′-CTTCATCTT CTAGCAAGAAGTAAAAGGCCTCGACACATACATAATAACT-3′, yielding VGp256. To generate GFP-tagged constructs, the GFP sequence was amplified from pKT128 (EUROSCARF Collection Center) with the primers 5′-GCGACGCGTTCTAAAGGTGAAGAATTATTC-3′ and 5′-GCGACGCGTTTTGTACAATTCATCCATACC-3′. The PCR product was cut with MluI and inserted into pMF616, NSp17, NSp20, NSp23, and VGp256 to yield NSp19 (GFP-Gas1*), LLp16 (GFP-Gas1), LLp17 (GFP-Gas1TMD), LLp18 (GFP-Gas1*TMD), and clone374 (GFP-Gas1*ΔTMD). To generate fusion constructs with CPY*, HA-Gas1* and HA-Gas1*TMD were first subcloned into pRS314 (*TRP1*, CEN) using XmaI and SacI, yielding VGp257 and VGp258. The coding sequence for 81 amino acids downstream of a unique BsrGI site in Gas1* was then removed in both constructs using PCR-based single primer site-directed mutagenesis and the primer 5′-CAAAGGAACAGCTATCTT TCTCCAGTTCTTCTTCTTCTTC-3′, leaving the coding region for the 57 C-terminal amino acids of HA-Gas1* and HA-Gas1*TMD, yielding clone390 and clone391. The CPY* moiety was amplified with PCR using the primers 5′-GCGCATATGTCATTGCAAAGACCGTTG-3′ and 5′-GCGTGTACATAAGGAGAAACCACCGTG-3′ from VGp173, cut with NdeI and BsrGI, and pasted into clone390 and clone391, yielding HA-CPY*GPI (clone392) and HA-CPY*TMD (LLp43). To obtain the GFP-tagged constructs, LLp18 was cut with MluI to release the GFP moiety. The fragment was purified, pasted into clone392 and LLp43, and cut with the same enzyme, yielding GFP-CPY*GPI (LLp47) and GFP-CPY*TMD (LLp45). To generate integrative plasmids containing these fusion constructs, they were subcloned into pRS306 using XmaI and SacI, yielding clone409 and clone410, respectively.

For lipidomics analysis, the various constructs expressing HA-tagged Gas1 derivatives together with the adjacent *URA3* gene were

amplified from the integrated plasmids using the primers 5′-CTGATA AAACAAAAACAACAAACACAGCTAAATCTCAACAATGTTGTT TAAATCCCTTTCD-3′ and 5′-CTCATCGAGCATCAAATGAAACTG CAATTTATTCATATCAGATTGTACTGAGAGTGCACC-3′. The PCR products were transformed into the *Δgas1* strain, replacing the *KANMX*6 cassette in the *GAS1* locus by homologous combination.

Antibodies

Primary antibodies for Western blotting and immunoprecipitation experiments were polyclonal rabbit antibodies from our laboratories (against Wbp1 and Gas1) and commercially available antibodies against HA or GFP (Roche). Secondary antibodies for Western blot analysis were peroxidase-coupled anti-mouse or anti-rabbit antibodies from Sigma-Aldrich.

CHX shut-off experiments

The experiments were started with exponentially growing cells in rich medium with an OD of 0.5 to 0.8. Translation was stopped by addition of CHX to a final concentration of 200 µg/ml. Equal-volume aliquots of cell culture were removed at indicated time points and moved to ice. Cells were lysed using 150 mM NaOH, followed by adding sample buffer containing 2% SDS and heating. Samples were analyzed by SDS-PAGE followed by Western blotting using the indicated primary antibodies, peroxidase-coupled secondary antibodies (Sigma-Aldrich), and ECL (Thermo Fisher Scientific) as substrate. Images were taken with a LAS-3000 mini-imaging system (Fujifilm), and bands were quantified using Multi-Gauge software (Fujifilm).

Fluorescence microscopy

Cells were grown overnight, diluted to OD 0.3, regrown for 4 h, washed with PBS, and immediately analyzed by fluorescence microcopy at RT. Cells were observed with an Olympus BX61 microscope equipped with a 100×/1.4 PlanApo oil-immersion lens and a conventional FITC cube as well as a DIC prism and polarizer for Nomarski imaging. Images were acquired using a DP70 camera and the DPcontroller software (Olympus).

Probing for GPI anchor attachment

20 OD of exponentially growing cells were lysed by bead beating in cold TEPI buffer in presence of 150 mM NaCl and protease inhibitor cocktail (Roche). 1 ml lysate was incubated with 1% of precondensed Triton X-114 (Fluka) at 4°C for 30 min with rotation and cleared by spinning at 14,000 *g* for 15 min at 4°C. Cleared lysates were split into two equal parts. One sample was incubated with 0.1 units PI-PLC (Thermo Fisher Scientific), and the second sample was mock-treated. Samples were incubated for 12 h at 4°C on a rocker. Phase separation was achieved by heating to 32°C followed by brief spinning. Phases were split, reextracted twice, and precipitated with trichloroacetic acid (TCA). Finally, SDS sample buffer containing 2% and 6 M urea was added, and samples were analyzed by SDS-PAGE and Western blotting.

GFP processing assay

Cells were grown overnight, diluted to OD 0.3, and regrown for 4 h. Before removal of aliquots, cells were incubated with CHX to a final concentration of 200 µg/ml and incubated for 15 min to allow for completion of posttranslational protein translocation across the ER membrane. Aliquots were removed, transferred to ice, lysed by alkaline treatment (Kushnirov, 2000), and resuspended in a cell density–normalized volume of loading buffer, followed by SDS-PAGE and Western blotting using anti-GFP antibody (Roche), HRP-conjugated anti-mouse secondary antibody (Sigma-Aldrich), and ECL as substrate. Images were taken with a LAS-3000 mini-imaging system, and bands were quantified using Multi-Gauge software.

Optiprep gradient flotation assay

10 OD of exponentially growing cells were harvested at OD 0.1, washed in ice cold water, and lysed by bead beating in TNE buffer (50 mM Tris-HCl, pH 7.4, 150 mM NaCl, and 5 mM EDTA) containing a protease inhibitor cocktail (Roche). The lysate was cleared, washed, and resuspended in 300 µl TNE buffer. Triton X-100 was added to 1% final concentration and incubated on ice for 30 min. Optiprep solution (Nycomed) was added to 40% final concentration, and the resulting solution was divided into two parts with equal volume. One part was considered "total"; the other part was overlaid with 1.2 ml of 30% Optiprep in TXNE (TNE with 1% Triton X-100) and finally with 200 µl TXNE. The samples were centrifuged at 55,000 rpm for 2 h in a TLS55 rotor (Beckman Coulter). Six fractions (360 µl each) were collected from top to bottom. Protein contents were precipitated by adding TCA to 15%, washed, and resuspended in SDS-PAGE loading buffer, followed by SDS-PAGE and Western blot analysis.

CoIP

200 ml of cell culture was grown to mid-log phase, washed, and lysed by bead beating with glass beads in lysis buffer (1× PBS, 1 mM EDTA, 1 mM PMSF, and protein inhibitor cocktail [Roche]). Lysates were cleared, solubilized by addition of 1% digitonin (EMD Millipore) for 30 min, and cleared by centrifugation for 20 min at 100,000 *g*, followed by incubation with magnetic beads (Thermo Fisher Scientific) coupled to rabbit IgG (Sigma-Aldrich) for 2 h at 4°C. Washing was done in lysis buffer with 0.5% digitonin followed by elution in SDS-loading buffer.

Lipid extraction protocols

Yeast culture, lipid extraction of sphingolipid and glycerophospholipids, and mass spectrometry analysis were performed as described (da Silveira Dos Santos et al., 2014). In brief, strains were grown in rich medium (yeast extract/peptone/dextrose) at 30°C to early exponential growth phase. 25 600-OD units were collected, and metabolism was stopped using TCA and cooling on ice. Samples were resuspended in extraction solvent (ethanol, water, diethylether, pyridine, and ammonium hydroxide). Internal standards were added, and the samples were broken through mechanical disruption using glass beads. Cell debris was pelleted by centrifugation, and the supernatant was collected. Lipid extract was divided into two aliquots for analysis of glycerophospholipids and sphingolipids. Mild alkaline hydrolysis was performed on the sphingolipid fraction. Finally, both fractions were desalted using water saturated *n*-butanol. Mass spectrometry analysis was done using direct infusion in negative and positive mode. The lipid species were identified by the *m*/*z* of the lipid and relevant fragment, and their amount was calculated by their signal intensities relative to the standards. Three independent biologic replicates were analyzed. The amount of ceramide and IPC species were summed to obtain the total amount of each lipid class, and the samples were normalized by the total amount of inorganic phosphate.

Determination of total phosphorus

Glycerophospholipid lipid extract was resuspended in 500 µl chloroform:methanol (1:1, vol/vol), and 50 µl was placed in 13-mm disposable Pyrex tubes. After solvent evaporation, 20 µl of water and 140 µl of 70% perchloric acid were added to the tubes. Samples were heated for 1 h at 180°C in a hood. Tubes were allowed to cool for 5 min at RT. Next, 800 µl of freshly prepared water:1.25% NH_4 molybdate: 1.67% ascorbic acid (5:2:1, vol/vol) was added to the tubes, followed by 5 min of heating at 100°C. Tubes were cooled at RT, and 100 µl was used for measurement of absorbance at 820 nm. A standard curve was generated with KH_2PO_4 standard solution and processed identically.

Online supplemental material

Fig. S1 shows the degradation rates of HA-Gas1* in single- and double-deletion mutants, highlighting the contribution of Hrd1-dependent ERAD to global protein degradation. Fig. S2 shows lipid profiles of *Δgas1* cells in dependence on expressing various Gas1* and Gas1 constructs along with control experiments. Table S1 shows a detailed list of yeast strains used in this study. Online supplemental material is available at http://www.jcb.org/cgi/content/full/jcb.201602010/DC1.

Acknowledgments

We thank the Jigami laboratory for plasmids and Martin Spiess and Robert Ernst for critical reading of the manuscript.

This work was supported by the Swiss National Center for Competence in Research (Chemical Biology) and the Schweizerischer Nationalfonds zur Förderung der Wissenschaftlichen Forschung to H. Riezman and the Ministerio de Ciencia e Innovación (BFU2009-07290 and BFU2014-59309-P) and the Junta de Andalucia (P09-CVI-4503) to M. Muñiz and V. Goder.

The authors declare no competing financial interests.

Author Contributions: N. Sikorska, L. Lemus, A. Aguilera-Romero, M. Muñiz, and V. Goder designed experiments. N. Sikorska, L. Lemus, A. Aguilera-Romero, J. Manzano-Lopez, and V. Goder performed experiments. N. Sikorska, L. Lemus, A. Aguilera-Romero, J. Manzano-Lopez, H. Riezman, M. Muñiz, and V. Goder evaluated data. V. Goder wrote the manuscript.

Submitted: 3 February 2016
Accepted: 26 May 2016

References

Arvan, P., X. Zhao, J. Ramos-Castaneda, and A. Chang. 2002. Secretory pathway quality control operating in Golgi, plasmalemmal, and endosomal systems. *Traffic.* 3:771–780. http://dx.doi.org/10.1034/j.1600-0854.2002.31102.x

Ashok, A., and R.S. Hegde. 2008. Retrotranslocation of prion proteins from the endoplasmic reticulum by preventing GPI signal transamidation. *Mol. Biol. Cell.* 19:3463–3476. http://dx.doi.org/10.1091/mbc.E08-01-0087

Bordallo, J., R.K. Plemper, A. Finger, and D.H. Wolf. 1998. Der3p/Hrd1p is required for endoplasmic reticulum-associated degradation of misfolded lumenal and integral membrane proteins. *Mol. Biol. Cell.* 9:209–222. http://dx.doi.org/10.1091/mbc.9.1.209

Braakman, I., and N.J. Bulleid. 2011. Protein folding and modification in the mammalian endoplasmic reticulum. *Annu. Rev. Biochem.* 80:71–99. http://dx.doi.org/10.1146/annurev-biochem-062209-093836

Carvalho, P., V. Goder, and T.A. Rapoport. 2006. Distinct ubiquitin-ligase complexes define convergent pathways for the degradation of ER proteins. *Cell.* 126:361–373. http://dx.doi.org/10.1016/j.cell.2006.05.043

Castillon, G.A., R. Watanabe, M. Taylor, T.M. Schwabe, and H. Riezman. 2009. Concentration of GPI-anchored proteins upon ER exit in yeast. *Traffic.* 10:186–200. http://dx.doi.org/10.1111/j.1600-0854.2008.00857.x

Castillon, G.A., A. Aguilera-Romero, J. Manzano-Lopez, S. Epstein, K. Kajiwara, K. Funato, R. Watanabe, H. Riezman, and M. Muñiz. 2011. The yeast p24 complex regulates GPI-anchored protein transport and quality control by monitoring anchor remodeling. *Mol. Biol. Cell.* 22:2924–2936. http://dx.doi.org/10.1091/mbc.E11-04-0294

Contreras, F.X., A.M. Ernst, P. Haberkant, P. Björkholm, E. Lindahl, B. Gönen, C. Tischer, A. Elofsson, G. von Heijne, C. Thiele, et al. 2012. Molecular recognition of a single sphingolipid species by a protein's transmembrane domain. *Nature.* 481:525–529. http://dx.doi.org/10.1038/nature10742

Copic, A., M. Dorrington, S. Pagant, J. Barry, M.C. Lee, I. Singh, J.L. Hartman IV, and E.A. Miller. 2009. Genomewide analysis reveals novel pathways affecting endoplasmic reticulum homeostasis, protein modification and quality control. *Genetics.* 182:757–769. http://dx.doi.org/10.1534/genetics.109.101105

da Silveira Dos Santos, A.X., I. Riezman, M.A. Aguilera-Romero, F. David, M. Piccolis, R. Loewith, O. Schaad, and H. Riezman. 2014. Systematic lipidomic analysis of yeast protein kinase and phosphatase mutants reveals novel insights into regulation of lipid homeostasis. *Mol. Biol. Cell.* 25:3234–3246. http://dx.doi.org/10.1091/mbc.E14-03-0851

Davidson, E.A., and D.C. Gowda. 2001. Glycobiology of *Plasmodium falciparum*. *Biochimie.* 83:601–604. http://dx.doi.org/10.1016/S0300-9084(01)01316-5

Drisaldi, B., R.S. Stewart, C. Adles, L.R. Stewart, E. Quaglio, E. Biasini, L. Fioriti, R. Chiesa, and D.A. Harris. 2003. Mutant PrP is delayed in its exit from the endoplasmic reticulum, but neither wild-type nor mutant PrP undergoes retrotranslocation prior to proteasomal degradation. *J. Biol. Chem.* 278:21732–21743. http://dx.doi.org/10.1074/jbc.M213247200

Fujita, M., and Y. Jigami. 2008. Lipid remodeling of GPI-anchored proteins and its function. *Biochim. Biophys. Acta.* 1780:410–420. http://dx.doi.org/10.1016/j.bbagen.2007.08.009

Fujita, M., and T. Kinoshita. 2012. GPI-anchor remodeling: Potential functions of GPI-anchors in intracellular trafficking and membrane dynamics. *Biochim. Biophys. Acta.* 1821:1050–1058. http://dx.doi.org/10.1016/j.bbalip.2012.01.004

Fujita, M., T. Yoko-O, and Y. Jigami. 2006. Inositol deacylation by Bst1p is required for the quality control of glycosylphosphatidylinositol-anchored proteins. *Mol. Biol. Cell.* 17:834–850. http://dx.doi.org/10.1091/mbc.E05-05-0443

Fujita, M., Y. Maeda, M. Ra, Y. Yamaguchi, R. Taguchi, and T. Kinoshita. 2009. GPI glycan remodeling by PGAP5 regulates transport of GPI-anchored proteins from the ER to the Golgi. *Cell.* 139:352–365. http://dx.doi.org/10.1016/j.cell.2009.08.040

Gatti, E., L. Popolo, M. Vai, N. Rota, and L. Alberghina. 1994. O-linked oligosaccharides in yeast glycosyl phosphatidylinositol-anchored protein gp115 are clustered in a serine-rich region not essential for its function. *J. Biol. Chem.* 269:19695–19700.

Gauss, R., T. Sommer, and E. Jarosch. 2006. The Hrd1p ligase complex forms a linchpin between ER-lumenal substrate selection and Cdc48p recruitment. *EMBO J.* 25:1827–1835. http://dx.doi.org/10.1038/sj.emboj.7601088

Goder, V., and A. Melero. 2011. Protein *O*-mannosyltransferases participate in ER protein quality control. *J. Cell Sci.* 124:144–153. http://dx.doi.org/10.1242/jcs.072181

Haynes, C.M., S. Caldwell, and A.A. Cooper. 2002. An HRD/DER-independent ER quality control mechanism involves Rsp5p-dependent ubiquitination and ER-Golgi transport. *J. Cell Biol.* 158:91–101. http://dx.doi.org/10.1083/jcb.200201053

Hirayama, H., M. Fujita, T. Yoko-o, and Y. Jigami. 2008. *O*-mannosylation is required for degradation of the endoplasmic reticulum-associated degradation substrate Gas1*p via the ubiquitin/proteasome pathway in *Saccharomyces cerevisiae*. *J. Biochem.* 143:555–567. http://dx.doi.org/10.1093/jb/mvm249

Jonikas, M.C., S.R. Collins, V. Denic, E. Oh, E.M. Quan, V. Schmid, J. Weibezahn, B. Schwappach, P. Walter, J.S. Weissman, and M. Schuldiner. 2009. Comprehensive characterization of genes required for protein folding in the endoplasmic reticulum. *Science.* 323:1693–1697. http://dx.doi.org/10.1126/science.1167983

Katiyar, S., G. Li, and W.J. Lennarz. 2004. A complex between peptide:N-glycanase and two proteasome-linked proteins suggests a mechanism for the degradation of misfolded glycoproteins. *Proc. Natl. Acad. Sci. USA.* 101:13774–13779. http://dx.doi.org/10.1073/pnas.0405663101

Kincaid, M.M., and A.A. Cooper. 2007. Misfolded proteins traffic from the endoplasmic reticulum (ER) due to ER export signals. *Mol. Biol. Cell.* 18:455–463. http://dx.doi.org/10.1091/mbc.E06-08-0696

Kushnirov, V.V. 2000. Rapid and reliable protein extraction from yeast. *Yeast.* 16:857–860. http://dx.doi.org/10.1002/1097-0061(20000630)16:9<857::AID-YEA561>3.0.CO;2-B

Loizides-Mangold, U., F.P. David, V.J. Nesatyy, T. Kinoshita, and H. Riezman. 2012. Glycosylphosphatidylinositol anchors regulate glycosphingolipid levels. *J. Lipid Res.* 53:1522–1534. http://dx.doi.org/10.1194/jlr.M025692

Ma, J., and S. Lindquist. 2001. Wild-type PrP and a mutant associated with prion disease are subject to retrograde transport and proteasome degradation. *Proc. Natl. Acad. Sci. USA.* 98:14955–14960. http://dx.doi.org/10.1073/pnas.011578098

Manzano-Lopez, J., A.M. Perez-Linero, A. Aguilera-Romero, M.E. Martin, T. Okano, D.V. Silva, P.H. Seeberger, H. Riezman, K. Funato, V. Goder, et al. 2015. COPII coat composition is actively regulated by luminal cargo maturation. *Curr. Biol.* 25:152–162. http://dx.doi.org/10.1016/j.cub.2014.11.039

Mayor, S., and H. Riezman. 2004. Sorting GPI-anchored proteins. *Nat. Rev. Mol. Cell Biol.* 5:110–120. http://dx.doi.org/10.1038/nrm1309

Mehnert, M., T. Sommer, and E. Jarosch. 2010. ERAD ubiquitin ligases: Multifunctional tools for protein quality control and waste disposal in the endoplasmic reticulum. *BioEssays.* 32:905–913. http://dx.doi.org/10.1002/bies.201000046

Meusser, B., C. Hirsch, E. Jarosch, and T. Sommer. 2005. ERAD: the long road to destruction. *Nat. Cell Biol.* 7:766–772. http://dx.doi.org/10.1038/ncb0805-766

Muñiz, M., C. Nuoffer, H.P. Hauri, and H. Riezman. 2000. The Emp24 complex recruits a specific cargo molecule into endoplasmic reticulum-derived vesicles. *J. Cell Biol.* 148:925–930. http://dx.doi.org/10.1083/jcb.148.5.925

Muñiz, M., P. Morsomme, and H. Riezman. 2001. Protein sorting upon exit from the endoplasmic reticulum. *Cell.* 104:313–320. http://dx.doi.org/10.1016/S0092-8674(01)00215-X

Petris, G., A. Casini, L. Sasset, F. Cesaratto, M. Bestagno, A. Cereseto, and O.R. Burrone. 2014. CD4 and BST-2/tetherin proteins retro-translocate from endoplasmic reticulum to cytosol as partially folded and multimeric molecules. *J. Biol. Chem.* 289:1–12. http://dx.doi.org/10.1074/jbc.M113.512368

Puig, B., H. Altmeppen, and M. Glatzel. 2014. The GPI-anchoring of PrP: Implications in sorting and pathogenesis. *Prion.* 8:11–18. http://dx.doi.org/10.4161/pri.27892

Reggiori, F., E. Canivenc-Gansel, and A. Conzelmann. 1997. Lipid remodeling leads to the introduction and exchange of defined ceramides on GPI proteins in the ER and Golgi of *Saccharomyces cerevisiae*. *EMBO J.* 16:3506–3518. http://dx.doi.org/10.1093/emboj/16.12.3506

Satpute-Krishnan, P., M. Ajinkya, S. Bhat, E. Itakura, R.S. Hegde, and J. Lippincott-Schwartz. 2014. ER stress-induced clearance of misfolded GPI-anchored proteins via the secretory pathway. *Cell.* 158:522–533. http://dx.doi.org/10.1016/j.cell.2014.06.026

Spear, E.D., and D.T. Ng. 2003. Stress tolerance of misfolded carboxypeptidase Y requires maintenance of protein trafficking and degradative pathways. *Mol. Biol. Cell.* 14:2756–2767. http://dx.doi.org/10.1091/mbc.E02-11-0717

Tashima, Y., R. Taguchi, C. Murata, H. Ashida, T. Kinoshita, and Y. Maeda. 2006. PGAP2 is essential for correct processing and stable expression of GPI-anchored proteins. *Mol. Biol. Cell.* 17:1410–1420. http://dx.doi.org/10.1091/mbc.E05-11-1005

Umemura, M., M. Fujita, T. Yoko-O, A. Fukamizu, and Y. Jigami. 2007. *Saccharomyces cerevisiae* CWH43 is involved in the remodeling of the lipid moiety of GPI anchors to ceramides. *Mol. Biol. Cell.* 18:4304–4316. http://dx.doi.org/10.1091/mbc.E07-05-0482

Vembar, S.S., and J.L. Brodsky. 2008. One step at a time: Endoplasmic reticulum-associated degradation. *Nat. Rev. Mol. Cell Biol.* 9:944–957. http://dx.doi.org/10.1038/nrm2546

Victoria, G.S., and C. Zurzolo. 2015. Trafficking and degradation pathways in pathogenic conversion of prions and prion-like proteins in neurodegenerative diseases. *Virus Res.* 207:146–154. http://dx.doi.org/10.1016/j.virusres.2015.01.019

Wang, S., and D.T. Ng. 2010. Evasion of endoplasmic reticulum surveillance makes Wsc1p an obligate substrate of Golgi quality control. *Mol. Biol. Cell.* 21:1153–1165. http://dx.doi.org/10.1091/mbc.E09-10-0910

Wang, Y.J., B.O. Tayo, A. Bandyopadhyay, H. Wang, T. Feng, N. Franceschini, H. Tang, J. Gao, Y.J. Sung, R.C. Elston, et al. COGENT BP consortium. 2014. The association of the vanin-1 N131S variant with blood pressure is mediated by endoplasmic reticulum-associated degradation and loss of function. *PLoS Genet.* 10:e1004641. http://dx.doi.org/10.1371/journal.pgen.1004641

Yedidia, Y., L. Horonchik, S. Tzaban, A. Yanai, and A. Taraboulos. 2001. Proteasomes and ubiquitin are involved in the turnover of the wild-type prion protein. *EMBO J.* 20:5383–5391. http://dx.doi.org/10.1093/emboj/20.19.5383

Zhao, Y., J.A. Macgurn, M. Liu, and S. Emr. 2013. The ART-Rsp5 ubiquitin ligase network comprises a plasma membrane quality control system that protects yeast cells from proteotoxic stress. *eLife.* 2:e00459. http://dx.doi.org/10.7554/eLife.00459